JOURNAL OF GEOPHYSICAL RESEARCH, VOL. 111, D12212, doi:10.1029/2005JD006774, 2006

Optical scattering patterns from single urban aerosol particles at Adelphi, Maryland, USA: A classification relating to particle morphologies

K. B. Aptowicz,[1,2] R. G. Pinnick,[3] S. C. Hill,[3] Y. L. Pan,[1] and R. K. Chang[1]

Received 10 October 2005; revised 12 February 2006; accepted 21 March 2006; published 28 June 2006.

[1] Angularly resolved elastic light scattering patterns from individual atmospheric aerosol particles (diameter 0.5–12 micrometers) sampled during fall (October 2004) at an urban site in the Baltimore-Washington metroplex are reported. These two-dimensional angular optical scattering (TAOS) patterns were collected for polar scattering angles θ varying from approximately 75° to 135° and azimuthal angles ϕ varying from 0° to 360°. Approximately 6000 scattering patterns were sampled over a span of 18 hours from an inlet located above our laboratory roof at Adelphi, Maryland. Our instrument recorded light scattering patterns of higher resolution and accuracy than have previously been achievable. The patterns suggest that background aerosol particles have diverse morphologies ranging from single spheres to complex structures. The frequency of occurrence of particle morphologies inferred from the TAOS patterns is strongly dependent on size. For nominally 1-μm particles, 65% appear spherical (or perturbed sphere) and only about 9% have complex structure (as suggested by their complex scattering features); whereas for nominally 5-μm particles, only 5% appear spherical (or perturbed sphere) and 71% appear to have complex structure. The patterns are quantitatively characterized using a degree of symmetry (Dsym) factor, calculated by examining both mirror and rotational symmetries in each pattern. In our measurements, atmospheric particles have two distinct populations: mostly micron-sized particles with Dsym values close to that of spheres and a population of mostly supermicron particles having a low but broad range of Dsym values. These observations are consistent with the commonly accepted notion that most micron-sized particles (in the accumulation mode) appear to be nearly spherical and are probably formed in the atmosphere through gas-particle reactions; whereas most supermicron particles appear to be nonspherical and are likely directly injected into the atmosphere. Our observations suggest that Lorenz-Mie theory may be adequate for most micron-sized particles but not for supermicron particles.

Citation: Aptowicz, K. B., R. G. Pinnick, S. C. Hill, Y. L. Pan, and R. K. Chang (2006), Optical scattering patterns from single urban aerosol particles at Adelphi, Maryland, USA: A classification relating to particle morphologies, *J. Geophys. Res.*, *111*, D12212, doi:10.1029/2005JD006774.

1. Introduction

[2] Aerosols are ubiquitous in the Earth's atmosphere, and their characterization is important in fields ranging from Earth climate to human health. For example, the analysis of airborne particulates helps elucidate the process of cloud formation, a critical link in the hydrological cycle [*Hirst et al.*, 2001], and provides insight into the atmospheric chemistry that determines the ultimate fate of pollutants.

[3] Extensive analyses of aerosol compositions have been made using many techniques over the last two decades; for example, by temperature and humidity controlled nephelometry [*Larson et al.*, 1982], temperature fractionation of aerosol particles [*Pinnick et al.*, 1987], pyrolysis and oxidation of carbon [*Dasch and Cadle*, 1989], X-ray dispersive analysis [*Sheridan et al.*, 1993], gas chromatography/mass spectrometry [*Rogge et al.*, 1993], ion exchange chromatography [*Decesari et al.*, 2002], pyrolysis gas chromatography/mass spectroscopy [*Gelencsér et al.*, 2002], X-ray fluorescence [*Chen et al.*, 2002], thermal-optical techniques [*Lim and Turpin*, 2002], laser ablation mass spectrometry [*Prather et al.*, 1994; *Lee et al.*, 2003; *Murphy et al.*, 2003; *Sullivan and Prather*, 2005], laser-induced fluorescence [*Pinnick et al.*, 1995; *Chang et al.*, 2005], laser-induced breakdown spectroscopy [*Hahn*, 1998; *Samuels et al.*, 2003], size exclusion chromatography/

[1]Department of Applied Physics and Center for Laser Diagnostics, Yale University, New Haven, Connecticut, USA.
[2]Now at Department of Physics, West Chester University, West Chester, Pennsylvania, USA.
[3]U.S. Army Research Laboratory, Adelphi, Maryland, USA.

0148-0227/06/2005JD006774$09.00

capillary electrophoresis [*Krivacsy et al.*, 2000], and epi-fluorescence microscopy/staining [*Bauer et al.*, 2002].

[4] Although significant advances have been made in determining the composition of aerosol particles, definitive characterization of their morphologies (in particular, their shape and internal refractive index distribution) remains elusive. One reason is that measuring 3-D morphologies of collected particles from single-view SEM images can be quite inaccurate, and finding these morphologies from multiple 2-D SEM images of the same particle taken at different angles is still an approximation and very tedious [*Hill et al.*, 1984]. Also, SEM images are sensitive only to surface morphology, not internal structure or variations in composition. More importantly, some particles contain volatile components (water, sulfuric and nitric acid, organic carbon compounds, etc.) and collection of particles, and subsequent examination by microscopy, scanning electron microscopy (SEM), or other means, might change their shape and internal structure.

[5] Elastic light scattering probes the morphological features of an aerosol in situ without changing the particle. In addition, elastic light scattering has a large scattering cross section, providing for a large signal, allowing for single particle analysis with relatively low illumination intensity, even in the submicrometer range. Furthermore, elastic light scattering is complementary to the techniques listed above. For example, when combined with Laser-Induced Fluorescence (LIF), another single-particle interrogation technique [*Pinnick et al.*, 2004], one has access to both the molecular composition of the particle (the existence and relative ratios of certain fluorophors), as well information on the shape, size, and internal structure of the aerosol particle. This complementary information provides a strong basis for classifying aerosol particles.

[6] The use of angularly resolved elastic light scattering to characterize aerosol particles has an extensive history. Over thirty years ago, Gucker and coworkers designed a device that could detect angularly resolved scattering light from aerosol in a laminar flow over almost a full 360° sweep of the polar angle (θ) range [*Gucker et al.*, 1973]. This device was used to determine the refractive index of polystyrene-latex spheres [*Marshall et al.*, 1976]. A few years later, *Bartholdi et al.* [1980] constructed a differential light scattering photometer using an elliptical reflector and array of 60 photodiodes to measure light scattered over polar angles 2.5–177.5° and spanning a large range of azimuthal angles. The differential light scattering detector (DAWN-A) developed by Wyatt and coworkers could detect light elastically scattered from particles in a flowing aerosol stream at sixteen angles simultaneously [*Wyatt et al.*, 1988]. The DAWN-A was used in a study to determine the fraction of spherical particles in ambient aerosols on the southwestern edge of the Great Smoky Mountains National Park near Townsend, Tennessee [*Dick et al.*, 1998; *Sachweh et al.*, 1995]. In that study, more than 90% of ambient particles in the 0.2–0.8 μm size range sampled from 15 July to 25 August 1995 were determined to be spherical.

[7] The apparatus used for the measurements reported here is similar in design to an apparatus introduced by *Kaye et al.* [1992]. In Kaye's pioneering work, a prolate ellipsoidal reflector collects light over a large solid angle (10.4 steradians) and reflects the scattered light onto a CCD detector. Using this instrument, particles of distinct shape (spheres, fibers, cubes, etc.) were analyzed by Kaye and coworkers and shown to qualitatively match predictions based on Lorenz-Mie theory and Rayleigh-Gans scattering [*Hirst and Kaye*, 1996]. Following Kaye's advancements, the authors of this paper developed a system to detect and compare the two-dimensional angular optical scattering (TAOS) patterns of aerosol particles. TAOS patterns of aggregates of Bacillus subtilis spores and polystyrene latex spheres [*Pan et al.*, 2003] were sufficiently different to be distinguished.

[8] However, several fundamental questions remain. What are the characteristics of elastic light scattering patterns from atmospheric aerosol particles, and what are possible particle morphologies? Further, given that elastic scattering patterns are dependent on particle size, internal refractive index distribution, and morphology, and given that there may not be a unique relation between scattering patterns and these particle parameters, what particle characteristics can be determined from scattering patterns? The technical challenges required to definitively answer these questions are difficult, and a definitive response has not been possible for several decades.

[9] To partially answer these questions, in the advancement described here, the TAOS setup described previously [*Pan et al.*, 2003] is integrated with an ambient aerosol sampling system and certain refinements are made in the optical system to improve the quality of the TAOS patterns (described below). Using this prototype TAOS system, 5993 patterns of atmospheric aerosol particles in the size range of 0.5 μm to 12 μm (light-scattering diameter) were captured over a period of about 18 hours. This paper discusses the apparatus used to collect the atmospheric aerosol scattering patterns, presents some initial qualitative and quantitative analysis of the patterns, and suggests some possible particle morphologies for the patterns.

2. Instrument to Measure TAOS

[10] The prototype instrument used to detect TAOS patterns of aerosol particles in situ is shown schematically in Figure 1a. To sample atmospheric aerosol, air was drawn through a metal duct protruding through the roof of our laboratory. A large squirrel cage (commercial chemical hood fan having 10 inch ducting) provided the aspiration for this duct. We want to sample particles in the 0.5–15 μm diameter range. Since supermicrometer-sized particles have a relatively low concentration in the atmosphere, an air-to-air concentrator (Dycor model XMX) was used to concentrate particles within a size range of 2–20 μm. (The concentrator works on the principle of virtual impaction, wherein inertia of particles causes them to cross fluid streamlines, allowing for separation of particles in a stagnation region where receiving tubes funnel particles to the minor exit flow of the concentrator.)

[11] Air from the duct was drawn at a rate of 770 L/min into the concentrator, and the concentrated particles were drawn from the minor exit flow of ~1 L/min. Smaller particles undergo almost no concentration, but pass unimpaired through the device. A large ballast tank (55 gallon drum with packing foam inserts) was installed between the virtual impactor concentrator and the concentrator pump to attenuate

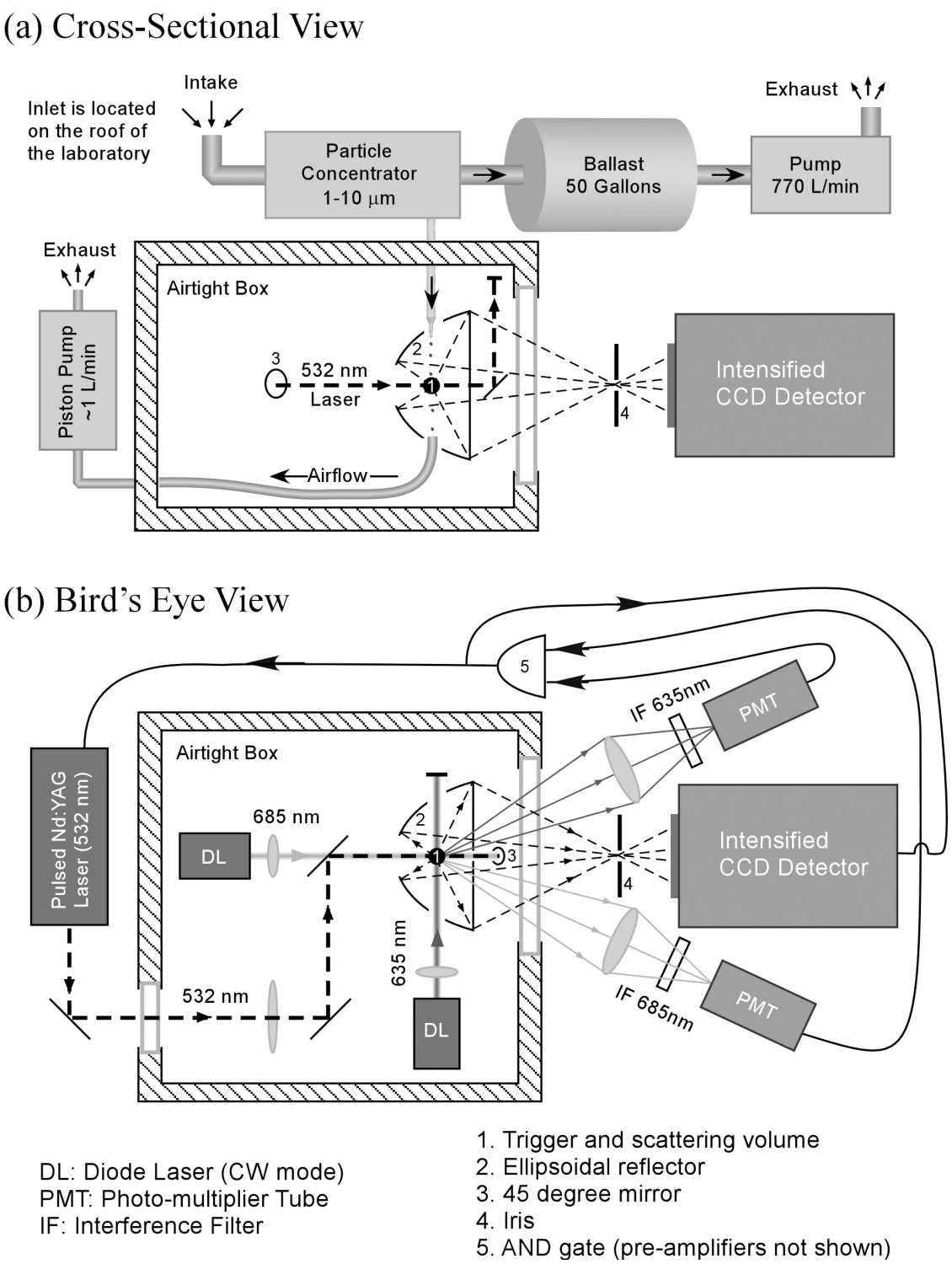

Figure 1. Diagram of TAOS instrument. (a) Cross-sectional view emphasizing aerosol handling and focusing. (b) Cross-beam optical triggering scheme and the ellipsoidal reflector for large solid angle light collection.

pressure fluctuations induced by the pump. The minor flow is drawn under slight negative pressure (about 2 millibar) into an airtight aluminum box (dimensions 18 in × 18 in × 18 in) through a conically shaped aerodynamic nozzle to achieve a focused laminar aerosol jet. The aerosol nozzle is positioned slightly above (∼0.5 cm) the scattering "focal volume" where the scattering measurement is made. The jet of aerosol exits the airtight box through an eduction tube positioned about 1 cm below the scattering focal volume. The eduction tube is connected through a second (smaller) air ballast to a constant-volume DC-motor-driven piston pump (KNF Neuberger, model UN05) that aspirates the box.

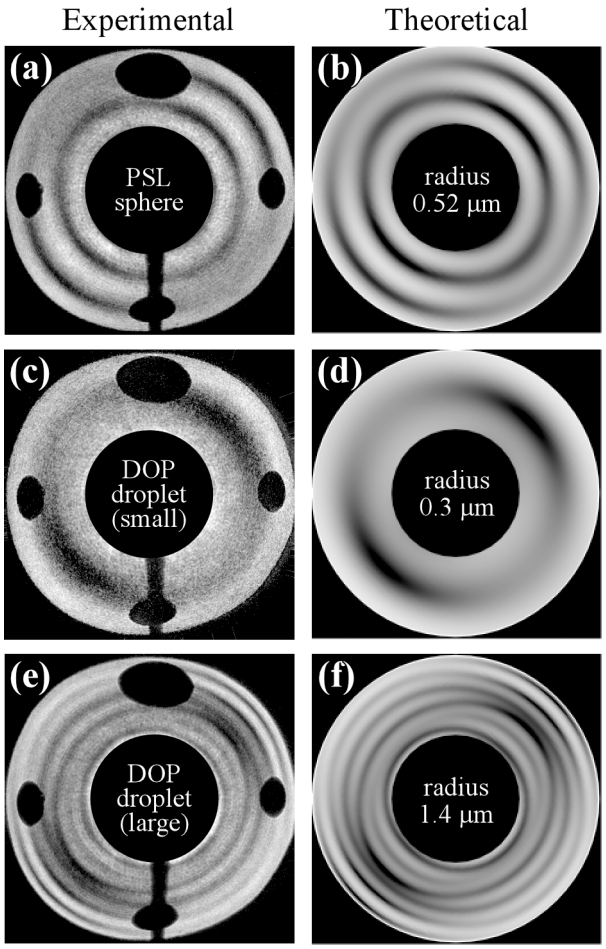

Figure 2. TAOS patterns of calibration particles compared with Lorenz-Mie calculations.

[12] Particles in the aerosol jet traverse the focal volume of a prolate ellipsoidal mirror (Opti-Forms Inc., Model E64-3) with major axis of 3.35″ and eccentricity of 0.75. Custom holes were drilled in the ellipsoid to gain access to the focal volume, as is evident in Figure 1. Light originating from a particle at the focal point of this mirror is reflected through a quartz window to the second focal point (and iris) located outside the box. The light rays from this ''virtual'' particle located at the iris are then detected by a 1024 × 1024 two-dimensional ICCD detector (Andor Technology, Model ISTAR DH734-25F-03), which can be considered to be located in the far-field by invoking the Fraunhofer approximation. By taking into account the geometry of the system, every pixel of the detector can be matched with a unique scattering angle (polar angle θ and azimuth angle ϕ). This geometry collects a large solid angle ($75° < \theta < 135°$, $0° < \phi < 360°$) of scattered light; however it suffers severely from the off-axis aberration coma that leads to uncertainty in labeling the scattering angle. A ray-tracing analysis of the system shows that for slight misalignment, the error in angle varies approximately as 1° for every 10 μm of particle misalignment (away from the mirror focal point) [*Aptowicz*, 2005]. The particle laden aerosol jet has a diameter of ~400 μm, which would lead to a severely distorted pattern.

[13] To alleviate this error, a cross-beam trigger system [*Pan et al.*, 1999] is incorporated into the optical train, as shown in Figure 1b. The two CW TEM00 diode lasers (Microlaser Systems), emitting light at 635 nm (power 25 mW) and 685 nm (40 mW), are focused with 7.5 cm and 5 cm focal length lenses to spot sizes 25 μm and 13 μm. Photomultiplier tubes (Hamamatsu model H6780-02) attached to long (16 cm) working distance microscope objectives detect the scattered light as the particle traverses the two beams. An interference filter is placed in front of each PMT so that it is only detecting the scattered light from a single diode-laser beam. The output from each PMT is amplified (EG&G Ortec 570, not shown) and passes to a discriminator (EG&G Ortec 850, not shown) to determine if a preset pulse-height threshold is met. The output of each analyzer is fed to a logic AND gate (EG&G Ortec CO4020). The AND gate output TTL pulse (for coincident scattering events) triggers both the pulsed laser source, a frequency-doubled Nd:YAG laser (Spectra Physics model X-30, 30 nsec pulse width), and the ICCD detector. The coincidence pulse also switches off the CW diode trigger beams, eliminating these unwanted signals from illuminating the ICCD during the ''on'' time.

[14] The crossed-diode-laser trigger system described above effectively reduces the errors due to off-axis aberrations, such as coma mentioned above, by limiting the sample volume to the volume defined by the crossed diode lasers (an ellipsoid with about 300 μm^2 cross section), which is considerably smaller than the aerosol jet. In actuality, the triggering volume is slightly above (~10 μm) the focal volume to account for delay times in the triggering sequence. The overall effective (size-dependent) sample rate for the TAOS sampling system peaks at about 12 liter/min for nominally 5 micron particles, decreasing to about 3 liter per/min for nominally 3 micron and 10 micron particles [see *Pinnick et al.*, 2004, Figure 2].

3. Collected TAOS Patterns

3.1. TAOS of Calibration Particles

[15] The prototype was first tested with calibration particles. Both individually dried polystyrene latex (PSL) spheres and dioctyl phthalate (DOP) droplets were aerosolized using a nebulizer (Royco Aerosol Generator, model 256) and fed into the inlet. TAOS patterns from these particles are shown in Figure 2. As is evident from the symmetry of the scattering patterns, the laser polarization is at $\phi = 45°$ clockwise rotation from vertical. The outer circumference of the image corresponds to light scattered at $\theta = 75°$ with respect to the laser beam's propagation axis (determined by the angular coverage of the ellipsoidal mirror); the inner circumference corresponds to light scattered at $\theta = 135°$ (determined by the size of the beam-steering mirror that blocks the green laser from the ICCD). There are several experimental artifacts embedded in the TAOS patterns. Holes drilled in the ellipsoidal mirror for one of the trigger beams as well as the particle-laden airstream appear as off-centered ovals in the patterns. A mounting post used to hold a beam-steering mirror appears as a black bar on the bottom of the image. The patterns are in good qualitative agreement with numerical simulations based on Lorenz-Mie theory.

3.2. TAOS of Atmospheric Aerosol

[16] We report here on approximately 6000 TAOS patterns of ambient aerosol particles collected overnight starting at 3 pm on 6 October and ending at 9 am on 7 October

2004. From a statistical perspective this data set is indeed meager. We have no evidence that the patterns would be repeated on different days, different seasons, or during different meteorological condition. Further measurements are needed to ascertain the generality of the patterns.

[17] The particles were sampled from a 15.2 cm diameter galvanized metal pipe extending 3 m above the (18 m high) roof of the U.S. Army Research Laboratory Harry Diamond Building in Adelphi, MD (Latitude 39°01′N, Longitude 76°57′W). Air mass back trajectories (last 24 hour) calculated with the NOAA ARL Hysplit model [*Draxler and Rolph*, 2003] reveal a change from north to southwest to west during the 18-hour measurement period.

[18] Twenty atmospheric aerosol TAOS patterns, captured sequentially, are shown in Figure 3. The intensity of the patterns is adjusted for ease of viewing. As is evident, there is a high level of particle-to-particle variability in the patterns. Some of the patterns are recognizable; for example images 1, 8, 15, and 20 are likely for spheres. Some patterns appear to arise from perturbed spheres, as suggested by their similarity to sphere-type patterns, whereas some patterns have similarities to those of fibers. Still other patterns have either blotchy islands, or swirl-like patterns of variable intensity and do not readily suggest particular particle shapes. In what follows, we describe how we analyzed these patterns for symmetry, visually classified the patterns into 5 groups, and then discuss the types of particles that may produce these different patterns.

4. Analysis and Visual Classification of the Atmospheric TAOS Data

4.1. Degree of Symmetry Analysis

[19] Previous efforts have been made to characterize elastic scattering patterns. In particular, scientists have investigated symmetries in scattering patterns as a means of classification. For example, Kaye et al. used three detectors at the same scattering angle (θ) but at three different azimuthal angles (ϕ = 0°, 120°, and 240°) to determine if circularly polarized input light was scattered symmetrically. From the three detectors, they determined an asymmetry factor that could be used to distinguish between different particle shapes. Similarly, *Dick et al.* [1998] introduced the sphericity index which is also based upon the symmetry of scattered light (eight detectors fixed at a single polar angle of 55° and spaced equally over azimuthal angles). Sampling ambient particles in the 0.2–0.8 μm size range, Dick found that greater than 90% of the particles were spherical. In this work, we introduce a degree of symmetry (Dsym) factor that quantifies the degree to which a TAOS pattern has rotational and mirror symmetries.

[20] Before determining Dsym, a mask is applied to each image to remove unwanted regions where experimental artifacts appear. The masked example TAOS pattern, shown in Figure 4a, is labeled matrix A. The rotational and mirror symmetries of this matrix are assessed using the following expression:

$$Dsym = \frac{1}{3}\sum_{i=1}^{3}\left(1 - \frac{\left(\sum_{pixel\ subset}(A - B_i)^2\right)^{1/2}}{2 \times RMS(A)}\right)$$

where B_1 is 180° rotation of matrix A (Figure 4b), and B_2 and B_3 are mirror images of matrix A (Figures 4c and 4d). Note the mirror symmetry planes were chosen to be parallel and orthogonal to the laser polarization. The root-mean-square (RMS) of matrix A is a normalization factor and the factor of 2 accounts for double counting. With this definition, the pattern of a spherical particle, which has a high degree of symmetry, would result in a Dsym value of 1 if there were no sources of optical aberrations or noise in the system.

[21] The Dsym values of the four data sets [PSL spheres (38 patterns), DOP droplets (169 patterns), and atmospheric particles (4244 patterns)] were calculated and are displayed in Figure 5. They are plotted with respect to the integrated scattering intensity of each pattern (which is related to particle size, see below). The size range of the particles, estimated from the DOP droplets, is 0.5 μm to 12 μm. The ceiling of 0.78 for the range of Dsym values (which should have limit 1) is due to noise and systematic sources of error in the apparatus, particularly distortions in the mirror surface (from a perfect ellipsoid) and variations in its reflectivity.

[22] The Dsym for PSL spheres range from 0.75 to 0.78 showing a high degree of symmetry as expected. The Dsym of DOP droplets varied from 0.60 to 0.78. Note in particular for DOP droplets the fall-off in Dsym for higher scattering intensities, corresponding to larger droplets. These particles have a higher spatial frequency of ring structure in the TAOS pattern, as depicted in Figure 2. For these larger particles, the slight distortions in the TAOS image due to the experimental setup (mainly imperfections in the mirror) led to distortion of these patterns and lower Dsym. As will be discussed in a later section, these distortions sabotage our ability to reliably determine particle refractive index.

[23] The Dsym for atmospheric aerosol TAOS patterns are widely distributed, ranging from 0.03 to 0.78. Two populations are clearly evident; a main population with Dsym values centered around 0.4, and another grouping of TAOS patterns with values in the 0.65 to 0.8 range, which we think indicates spherical or near-spherical particles, except in the unlikely case of a rotationally symmetric particle that has the axis of rotation aligned with the major axis of the ellipsoidal mirror. The particles with a high Dsym have primarily low scattering intensities, suggesting that the concentration of spherical particles increase as the size of the particles decrease. This point is pursued further in the next section.

4.2. Visual Classification of Scattering Patterns and Possible Particle Morphologies

[24] To examine more carefully the scattering pattern characteristics, 2525 patterns (about 500 patterns from five different scattering intensity ranges) were sorted. Because a rigorous image analysis routine was not available, we were forced to rely on the human eye to visually sort the complex patterns (requiring about 30 hours RGP time). Examples of some patterns that fit into the five classes into which we sort are shown in Figure 6. Figure 6 is a collection of 15 patterns representing 5 different classes (denoted sphere, perturbed sphere, swirl, fiber, and complex structure) spanning 3 size ranges.

[25] To estimate the relation between particle size and scattered intensity for our experimental arrangement, we

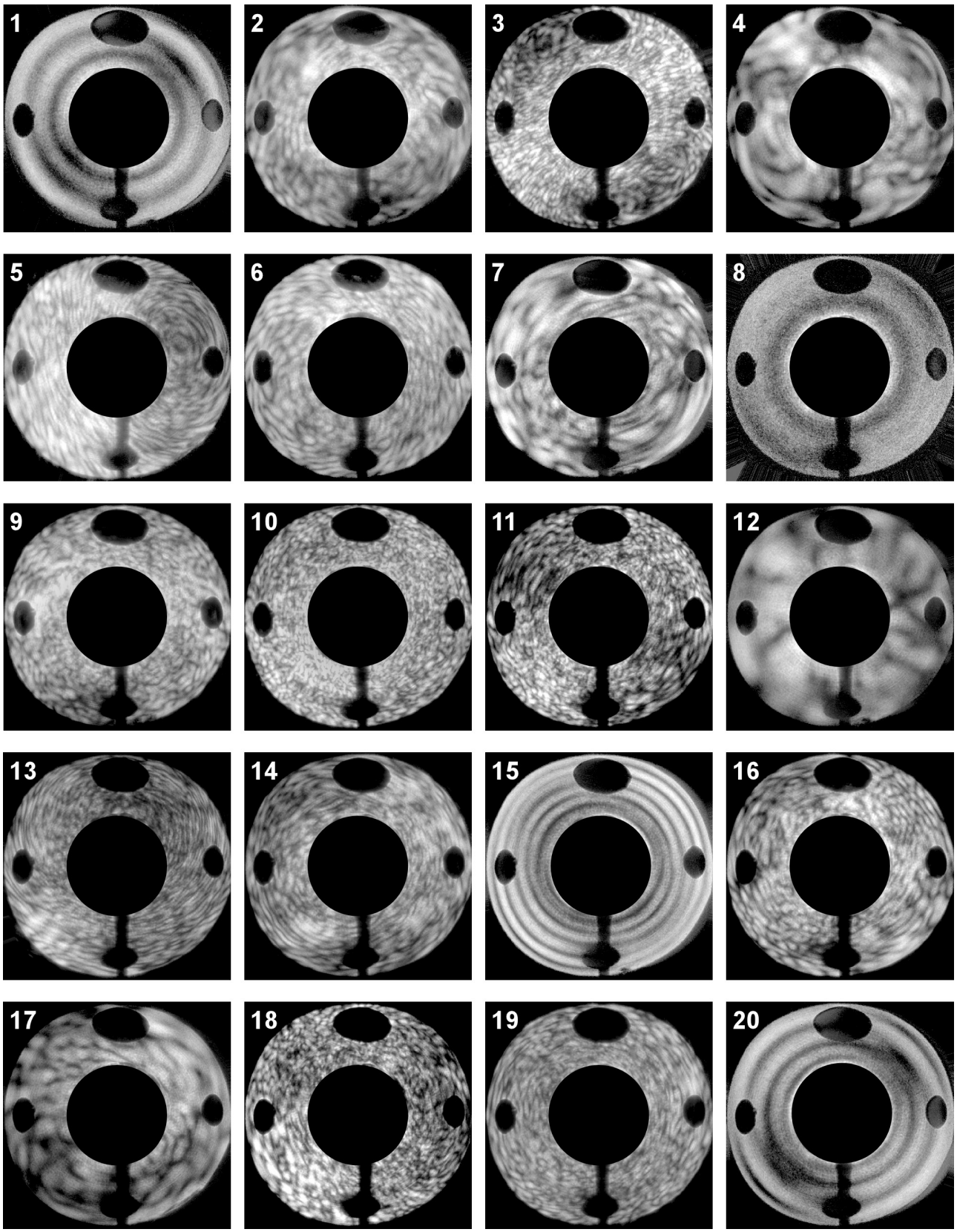

Figure 3. Twenty consecutive TAOS patterns of ambient particles captured during data collection run.

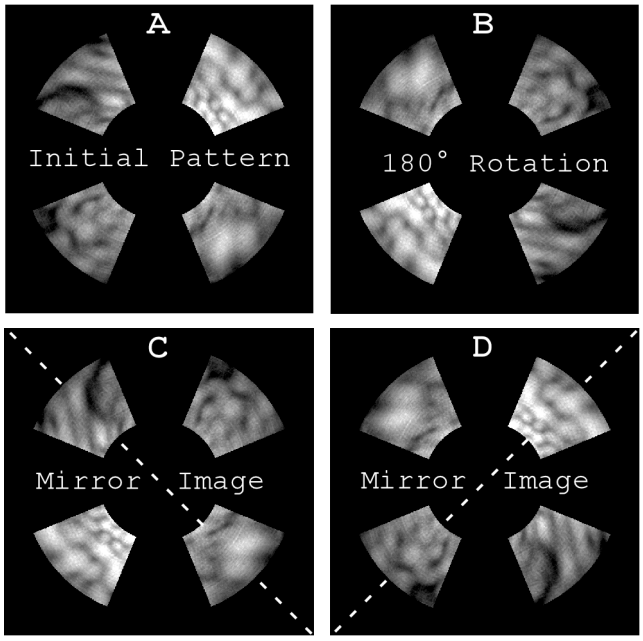

Figure 4. Pattern manipulations to determine Dsym value. (a) Initial pattern, (b) the pattern if the initial pattern is rotated about the center point by 180°, and (c and d) the resultant patterns if the initial pattern is transposed about the lines shown.

calculated, as a function of the diameter (d) of the sphere, the scattering intensity integrated over azimuthal angle ϕ from 0 to 360°, and polar angle θ from 85 to 128°, using separation of variables [*Barber and Hill*, 1990]. We ignored holes in the mirror. In addition, we assumed that this relation of integrated scattering to size was the same for all particles, no matter how nonspherical and no matter what the orientation. This approximation cannot be valid, in general, for real nonspherical particles, but does give a rough approximation of particle size. The result, in Figure 7, illustrates that the mapping from measured intensity to diameter of a sphere is not unique. The uncertainty in size determined from the scattered intensity is relatively large (about a factor 2). Also, if the uncertainty of the refractive index is taken into account, the uncertainty grows even larger. Nonetheless, such a calculation does give an approximate size.

[26] We should note there is an additional uncertainty in our size selection criteria introduced by our use of a virtual impactor and focusing nozzle in the aerosol sampling system, since the sample rate for this system is dependent on aerodynamic size, not light-scattering size.

[27] Below are descriptions of the different pattern classes as well as possible characteristics of the aerosol.

4.2.1. Spherical Particles

[28] TAOS patterns resulting from particles believed to be spherical are shown in the first row of Figure 6. These patterns have a characteristic ring-like structure, as can be calculated from Lorenz-Mie theory. The Dsym for these patterns are 0.77 for the nominally 1-μm sphere, 0.72 for the 3-μm sphere, and 0.60 for the 5-μm sphere. Candidate particles for these spherical patterns include the following:

[29] 1. The first group of candidates includes both primary and secondary (formed by atmospheric gas-to-particle reactions) organic carbon particles including single-ring, double-ring, and polycyclic aromatic hydrocarbons, carboxylic acids, organic polymers, humic acids, fulvic acids and humic-like substances [*Mukai and Ambe*, 1986; *Rogge et al.*, 1993; *Saxena and Hildemann*, 1996; *Zappoli et al.*, 1999; *Krivacsy et al.*, 2000; *Decesari et al.*, 2002; *Kiss et al.*, 2002; *Gelencsér et al.*, 2002; *Pinnick et al.*, 2004]. (We note that *Chen et al.* [2002] report that carbonaceous material accounts for 30–45% of the PM 2.5 mass in the Baltimore-Washington corridor, and that a large fraction likely derives from internal combustion engine emissions. Also, *Lee et al.* [2003] found that, in Atlanta, 45% of particles in the 0.35–2.5 μm diameter range contained organic carbon.)

[30] 2. The second group of candidates includes aqueous mixtures of inorganic salts including sulfates, nitrates, chlor-

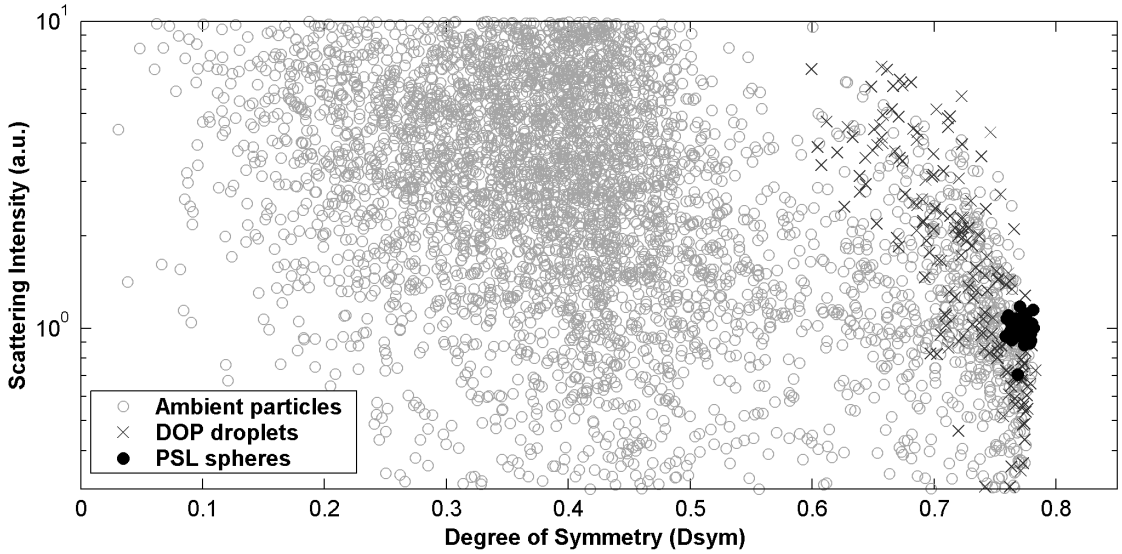

Figure 5. Degree of symmetry (Dsym) versus integrated scattering intensity, which roughly correlates to particle size, for calibration and ambient particles.

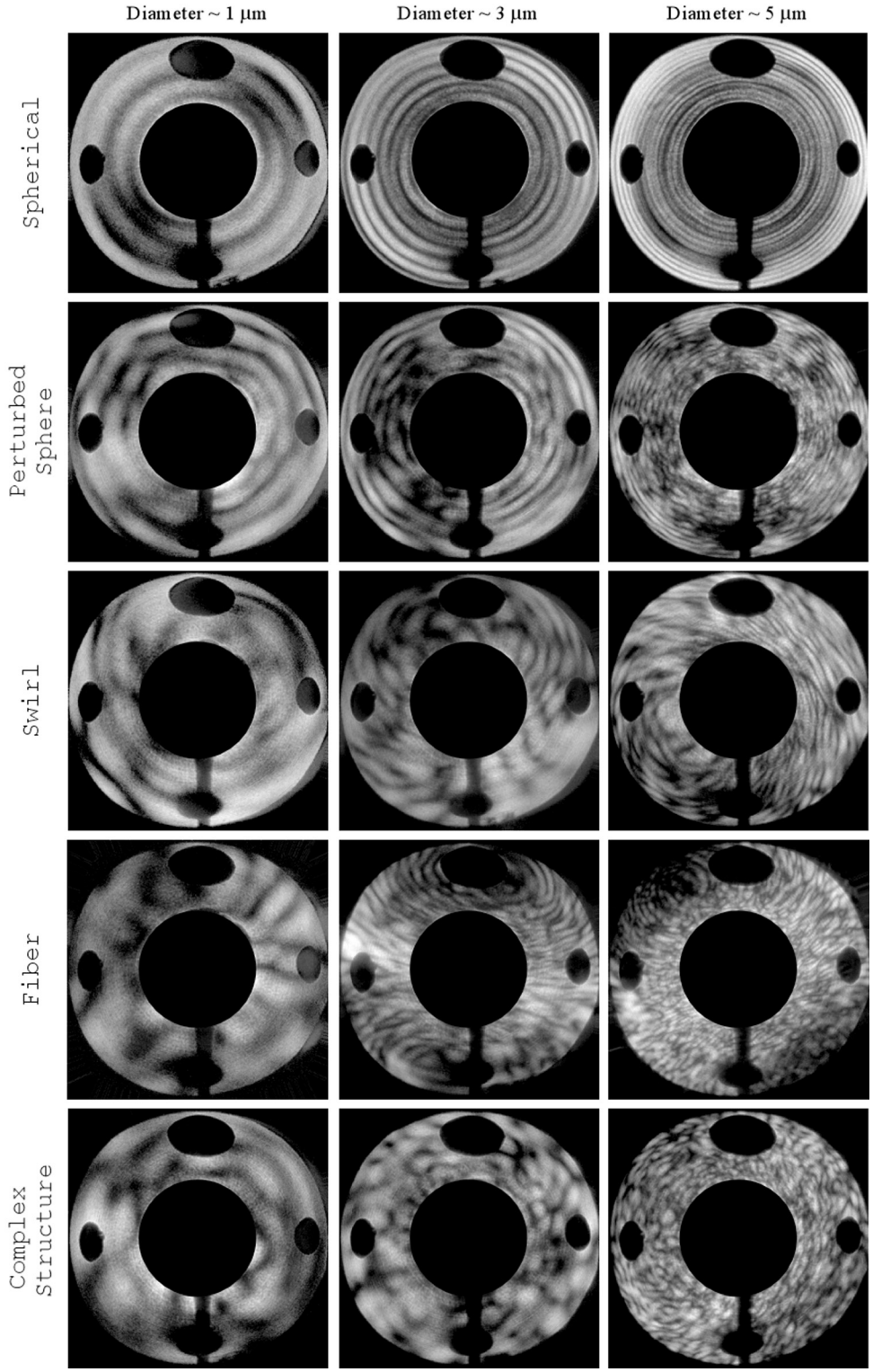

Figure 6. Qualitative classification of TAOS patterns depicting the variability of atmospheric particle scattering patterns.

ides, sulfites, and carbonates [*Prospero et al.*, 1983; *Kopcewicz et al.*, 1991; *Charlson and Wigley*, 1994], methane sulfonic acid [*Qian and Ishizaka*, 1993], sea salt aerosol containing sea salts and water [*Prospero et al.*, 1983]. (We note that aqueous mixtures of ammonium sulfate, ammonium bisulfate, and sodium chloride remain liquid at relative humidities as low as 79%, 39%, and 76% [*Tang*, 1976; *Tang and Munkelwitz*, 1977; *Tang et al.*, 1977; *Cziczo et al.*, 1997], and that relative humidities for the air masses sampled at the site ranged from 42 to 58% during the sampling period.)

[31] 3. Some coal and oil fly ash particles [*Mamane et al.*, 1986], amorphous carbonaceous tar balls [*Pósfai et al.*,

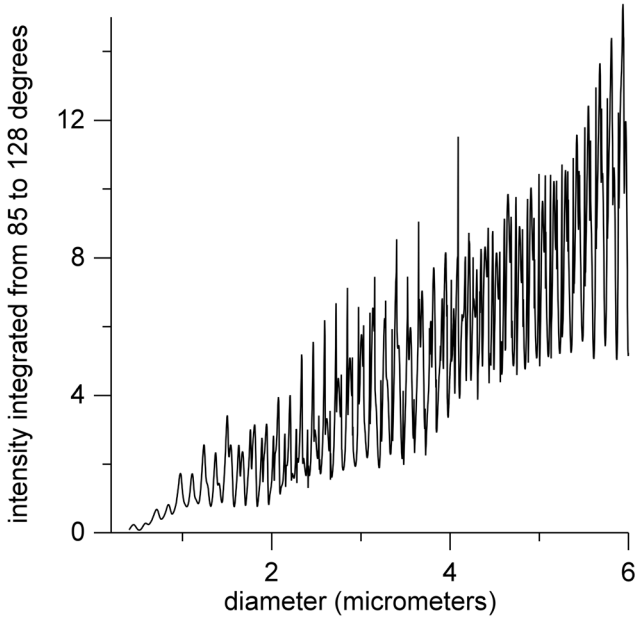

Figure 7. Calculated intensity (arbitrary units) scattered by a sphere versus diameter of the sphere. The intensity is integrated over all azimuthal angles and over the polar scattering angle (θ) between 85 and 128°. The refractive index is 1.48.

2004]; and silicate and iron oxide spheres [*Ebert et al.*, 2002] are also possible candidates for the spherical particle class.

4.2.2. Perturbed Spheres

[32] TAOS patterns in the second row of Figure 6 have a deformed or broken ring-like structure suggestive of a slightly perturbed spherical particle, for example a slightly rough sphere, a sphere having small particles on its surface, a slightly nonspherical particle (either homogeneous or of mixed composition), or a sphere containing small inclusions [*Videen et al.*, 2000]. Possible atmospheric particles for these patterns may include (1) multicomponent particles such as organic carbon with sulfates, organic carbon with nitrates, organic carbon with crustal material, organic carbon with black carbon inclusions, organic carbon with sulfuric acid, water soluble organic carbon with nonwater soluble organic carbon, acid sulfate particles with black carbon inclusions, metal inclusions in sulfuric acid, silicate fly ash, sulfuric acid mixed with crustal material, and smoke from biomass burning and internal combustion engines [*Mamane et al.*, 1986; *Novakov and Penner*, 1993; *Lee et al.*, 2002; *Ebert et al.*, 2002; *Lim and Turpin*, 2002]; (2) neutralized acid sulfates [*Sheridan et al.*, 1993]; and (3) nearly spherical pollens or spores [*Ebert et al.*, 2002].

[33] We note as an aside that the possibility of perturbed sphere (or any nonsphere) patterns resulting from there being two particles in the sensing volume is tiny, since the sensing volume is only about 4×10^{-12} liter and aerosol concentrations (enhanced by the virtual impactor) should not exceed about 10^5 particles per liter for 1–10 micron particles.

4.2.3. Swirl Patterns

[34] The TAOS patterns in the third row of Figure 6, labeled "swirl" patterns, are of unknown origin. The swirl patterns seem to be composed of broken or twisted rings; however the rings are off center. This is not due to the aberration coma, which would lead to the squeezing or spreading of pattern features. The patterns have some similarity to those for droplets with inclusions (perhaps having inclusions larger than those for perturbed spheres) or deformed droplets [*Secker et al.*, 2000], multiplet particles [*Ashkin and Dziedzic*, 1980; *Kaye et al.*, 1992], fiber clusters, and flake particles [*Kaye*, 1998]. Candidate particles that may produce the patterns are (1) the mixtures suggested for the perturbed sphere class but with more nonhomogeneity, (2) crystalline-like leaf surface waxes dislodged by the wind or by rubbing motions of leaves against each other [*Rogge et al.*, 1993], (3) multiplet particles, (4) sea salt crystals [*Ebert et al.*, 2002], (5) silica shards produced by the combustion of coal [*Rietmeijer and Janeczek*, 1997], and (6) crystalline particles of quartz or clay minerals [*Ebert et al.*, 2002].

4.2.4. Fiber-Like Particles

[35] The TAOS patterns in the fourth row of Figure 6 are characteristic of fibers [*Kaye*, 1998; *Kaye et al.*, 1992], or doublet particles of similar size [*Kaye et al.*, 1992]. These patterns might be attributable to fiber-like particles (possibly ammonium nitrate crystals, as found by *Kopcewicz et al.* [1991], rod-like bacterial endospores [*Shaffer and Lighthart*, 1997], and tire debris (owing to the heavy traffic in the Maryland locale), or possibly by doublet particles (particles stuck together) of the same or different composition but with similar size.

4.2.5. Particles of Complex Structure

[36] The final row of Figure 6 shows TAOS patterns composed primarily of islands where the orientation of the islands does not appear to be strongly correlated to any particular direction. These patterns look similar to those captured previously for aggregates [*Pan et al.*, 2003], and to kaolin, Arizona road dust, and to dried droplets containing ammonium sulfate, sodium chloride, or bovine albumin [see *Aptowicz*, 2005]. The test particle results suggest that the particles corresponding to these patterns have a complex structure, and may be aggregates. Candidate atmospheric particles that may produce these patterns are (1) mineral dust of soil origin; (2) biological particles with complex morphology that are injected directly into the atmosphere including fragments of skin, leaves, bark, pollens, plant spores, algae, and fungi [*Jaenicke*, 2005]; (3) particles composed of water soluble materials (e.g., salts) that have formed from droplets that dried in such a way that the resulting dry particles were not spherical; (4) agglomerates of particles of the same composition (e.g., aggregated mineral dust of soil origin [*Ebert et al.*, 2002; *Pinnick et al.*, 1985]), carbonaceous chain aggregates [*Sheridan et al.*, 1993] including aggregate soot particles from oil-fired or coal-fired power plants [*Chylek et al.*, 1981; *Ebert et al.*, 2002], and diesel engine emissions [*Huang et al.*, 1994]; and (5) agglomerates of particles of different composition that may include sulfates, nitrates, quartz, clay minerals, organic carbon, black carbon [*Ebert et al.*, 2002], or materials of biological origin.

4.3. Frequency of Occurrence of Pattern Classes

[37] To investigate the frequency of occurrence of the various scattering patterns as a function of particle size,

Table 1. Frequency of Occurrence of Ambient Aerosol Scattering Pattern Class Types for Several Particle Sizes

	Total Particles Analyzed	Spheres,[a] %	Perturbed Spheres,[a] %	Swirls,[b] %	Fiber,[b] %	Complex Structure,[b] %
Intensity ~ 0.5 (nominally 0.5 μm)	460	42	17	26	5	10
Intensity ~ 1 (nominally 1 μm)	523	42	23	22	5	9
Intensity ~ 2 (nominally 2 μm)	505	21	24	26	4	25
Intensity ~ 4 (nominally 3 μm)	527	6	13	32	6	43
Intensity ~ 8 (nominally 5 μm)	510	<0.1	5	18	6	71

[a]Most particles in these columns are likely formed by gas-to-particle reactions in the atmosphere.
[b]Most particles in these columns are likely injected directly into the atmosphere.

subsets of the data ensemble were sorted according to particle scattering intensity integrated over all measured angles. The result (Table 1) reveals a marked decrease in the fraction of spheres (from 42% to <0.1%) as particle size increases from nominally 0.5 μm to 5 μm (light scattering diameter). The fraction of perturbed spheres also decreases with increasing size, although not as much (from 17% to 5%). The fraction of swirl-like and fiber-like patterns do not vary much with size. On the other hand, there is a significant increase in the number of complex structure particle patterns with increasing size; from 10% to 71%.

[38] These findings are consistent with the idea that micron-sized particles are primarily liquid, and are formed mainly by heterogeneous nucleation gas-to-particle reaction processes in the atmosphere [*Weiss et al.*, 1977; *Odum et al.*, 1996; *Novakov et al.*, 1997; *Prospero et al.*, 1983; *Lim and Turpin*, 2002; *Gelencsér et al.*, 2002; *Decesari et al.*, 2002; *Sullivan and Prather*, 2005], whereas most supermicron particles are directly injected into the atmosphere from a variety of sources [*Prospero et al.*, 1983; *Jaenicke*, 2005; *Sullivan and Prather*, 2005], or may be formed by agglomeration of smaller particles in the atmosphere.

4.4. Refractive Index Determinations for Spherical Particles

[39] We attempted to invert the spherical class of TAOS patterns to determine particle diameter and refractive index. However, the quality of the patterns (as the Dsym values for polystyrene and DOP suggest) are significantly degraded by distortions in the elliptical mirror surface and by variations in its reflectivity. The patterns were not of sufficiently quality to be inverted, except for a small number (about 3%) of patterns from relatively small particles.

[40] To determine the most likely diameter d and the refractive index m for each of the spherical atmospheric particles, we used a Levenburg-Marquardt optimization program [*Press et al.*, 1992]. This routing found the d and m that give calculated (with separation of variables) TAOS patterns that best fit the measured TAOS patterns.

[41] The merit function for this analysis was defined as

$$\chi^2 = \frac{1}{N}\sum_m \sum_n \left(\frac{I_{\exp}(\theta_n, \phi_m) - I_{theory}(\theta_n, \phi_m)}{\sigma(\theta_n, \phi_m)} \right)^2,$$

where $I_{exp}(\theta_n)$ is the experimental intensity value and $I_{theory}(\theta_n)$ is the intensity value based on Lorenz-Mie theory, θ_n is the scattering angle, $\sigma(\theta_n)$ is the estimated standard deviation at that angle, and N is the total number of points compared. Only the scattering planes perpendicular and parallel to the input polarization were compared, thus the azimuthal angle ϕ_m was set to 0°, 90°, 180° and 270°. For the scattering angle θ_n, fifty angles equally distributed between 81° and 128° were selected. The experimental data were binned over approximately 4 pixels to filter out the higher spatial frequency noise. Two factors were accounted for to estimate $\sigma(\theta_n)$: (1) ICCD associated noise and (2) fluctuations in intensity due to distortions in the ellipsoidal mirror.

[42] In Figure 8, the best fit parameters found are shown for PSL spheres, DOP droplets, and the atmospheric particles. Since the index of refraction of PSL and DOP is known, these data sets can be used to estimate the accuracy and the precision of this analysis. A summary of the results is shown Table 2. Of the 587 atmospheric TAOS patterns in the sphere class, only 17 patterns matched well with Lorenz-Mie theory. For these patterns, the real index of refraction ranged from 1.40 to 1.58. The mean refractive index of the ambient aerosols (1.49) is 2σ from the refractive index of water.

[43] Because the overall distortion and noise was such that only 3% of the spherical particles matched well with calculated patterns, we lack confidence that values of d and m deduced by our inversion are representative of atmospheric particles in the spherical class. However, we note that the values of m deduced are in the range of m found for

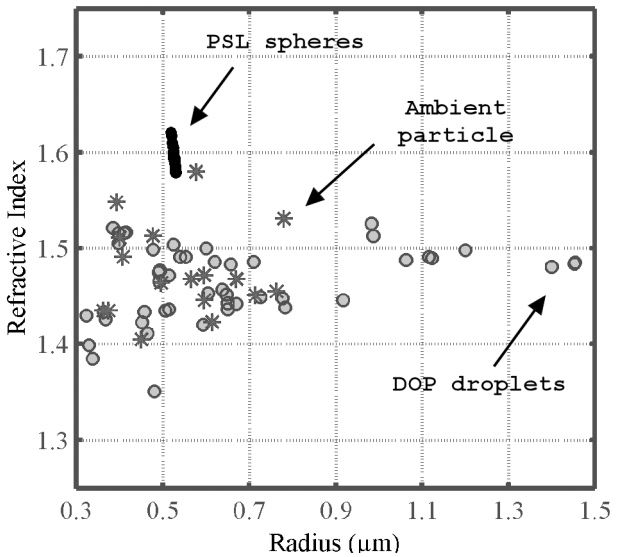

Figure 8. Best fit diameter and refractive index values matched to Lorenz-Mie theory. The ambient particles selected for these data have TAOS pattern of circular or nearly circular rings.

Table 2. Found Refractive Index of Spherical Aerosols

	Matching Patterns	Mean Refractive Index	Standard Deviation
PSL spheres	38	1.597	0.009
DOP droplets	44	1.47	0.03
Atmospheric aerosol	17	1.49	0.08

compounds known to be in atmospheric aerosol. A large variety of organic and inorganic compounds have been measured in atmospheric aerosol [see, e.g., *Seinfeld and Pandis*, 1998, pp. 709–749, and references therein]. Probably most atmospheric droplets that contain organic carbon contain many types of compounds.

[44] The data presented here suggest that with a better quality elliptical mirror and with a third diode laser for measuring the light-scattering particle size, it may be possible to obtain measurements of particle number as a function of particle refractive index. Such data could be used, e.g., in studying atmospheric chemistry, to determine if the particle number vs. refractive index is consistent with models of reactions within and on the surface of droplets in the atmosphere. The data presented here also suggest that with more rapid data collection (e.g., using orthogonal linear arrays), and with particle sorting technology [*Pan et al.*, 2004], it may be possible to collect the particles in different refractive index categories so that the particles in each category could be analyzed separately.

5. Summary

[45] High-resolution angular scattering patterns of nearly 6000 atmospheric aerosol particles have been measured during an 18-hour period in early October 2004 in the Baltimore-Washington urban metroplex. Particle morphologies for these patterns range from homogeneous spheres to perturbed spheres to what appear to be particles of complex shapes, including nonspherical aggregates. Particle morphologies are highly dependent on size. For nominally 1-μm particles, 65% are spherical (or perturbed sphere), and only 9% have a complex structure; whereas for nominally 5-μm particles, only 5% are spherical (or perturbed sphere), and 71% have a complex structure. The dominance of spherical (or near-spherical) particles in the 1 μm population is consistent with the notion that the majority of these particles being formed in the atmosphere by nucleation and gas-to-particle reaction processes. The larger, supermicron particle population has few spherical (or perturbed sphere) particles and are probably injected directly into the atmosphere.

[46] These findings suggest that, for urban aerosols in the Baltimore-Washington area in early October, Lorenz-Mie theory may be an adequate (depending upon the application) scattering model for most micron-sized particles, but may be inadequate for supermicron particles. Fitting a small number of atmospheric TAOS patterns for spherical particles revealed best fit refractive index values in the range 1.4 to 1.6.

[47] Elastic light scattering patterns are sensitive to particle size, shape, internal structure, and composition. However, the inverse problem of determining the particle morphology from the TAOS is extremely complex, especially for atmospheric particles where there are so many types of morphologies. Although the inverse problem is extremely difficult in the general case, clearly it can be useful to make correlations between test particles and TAOS patterns, and then use this information (possibly stored, e.g., as sets of neural network coefficients) to classify atmospheric TAOS patterns. For further progress to be made, it will be essential to use a better quality ellipsoidal mirror to obtain better quality scattering patterns and to develop computer algorithms and code to make a more rigorous classification of the particle scattering patterns.

[48] **Acknowledgments.** This research was supported by the DTRA Rapid Aerosol Agent Detection program, the DARPA Spectral Sensing of Bio-Aerosols program, the DARPA Short UV Optical Sources program, and Army Research Laboratory mission funds. K. Aptowicz was supported by a Sandia National Labs Excellence in Engineering Fellowship. John Bowersett, R.T. White, and Clyde Stup (Army Research Lab) machined the various aerosol nozzles, optics holders, and the air-tight box for the TAOS system. Dennis Martin (ARL) did the electrical design and wiring. The raw TAOS data files (about 20 Gigabytes) can be obtained (by supplying an external hard drive) from K.B.A. (kaptowicz@wcupa.edu) or R.G.P. (rpinnick@arl.army.mil).

References

Aptowicz, K. B. (2005), Angularly-resolved elastic light scattering of micro-particles, Ph.D. thesis, 28 pp., Yale Univ., New Haven, Conn.

Ashkin, A., and J. M. Dziedzic (1980), Observation of light scattering from nonspherical particles using optical levitation, *Appl. Opt.*, *19*(5), 660–668.

Barber, P. W., and S. C. Hill (1990), *Light Scattering by Particles: Computational Methods*, World Sci., Hackensack, N. J.

Bartholdi, M., G. C. Salzman, R. D. Hiebert, and M. Kerker (1980), Differential light scattering photometer for rapid analysis of single particles in flow, *Appl. Opt.*, *19*(10), 1573–1581.

Bauer, H., A. Kasper-Giebl, M. Loflund, H. Giebl, R. Hitzenberger, F. Zibuschka, and H. Puxbaum (2002), The contribution of bacteria and fungal spores to the organic carbon content of cloud water, precipitation and aerosols, *Atmos. Res.*, *64*, 109–119.

Chang, R. K., Y.-L. Pan, R. G. Pinnick, and S. C. Hill (2005), Method and instrumentation for measuring fluorescence spectra of individual airborne particles sampled from ambient air, Patent 6,947,134 B2, U.S. Patent and Trademark Off., Washington, D. C., 20 Sep.

Charlson, R. J., and T. M. L. Wigley (1994), Sulfate aerosol and climate change, *Sci. Am.*, *270*(2), 28–35.

Chen, L.-W. A., B. G. Doddridge, R. R. Dickerson, J. C. Chow, and R. C. Henry (2002), Origins of fine aerosol mass in the Baltimore-Washington corridor: Implications from observation, factor analysis, and ensemble air parcel back trajectories, *Atmos. Environ.*, *36*, 4541–4554.

Chylek, P., V. Ramaswamy, R. Cheng, and R. G. Pinnick (1981), Optical properties and mass concentration of carbonaceous smokes, *Appl. Opt.*, *20*(17), 2980–2985.

Cziczo, D. J., J. B. Nowak, J. H. Hu, and J. P. D. Abbatt (1997), Infrared spectroscopy of model tropospheric aerosols as a function of relative humidity: Observation of deliquescence and crystallization, *J. Geophys. Res.*, *102*(D15), 18,843–18,850.

Dasch, J. M., and S. H. Cadle (1989), Atmospheric carbon particles in the Detroit urban area: Wintertime sources and sinks, *Aerosol Sci. Technol.*, *10*, 236–248.

Decesari, S., M. C. Facchini, E. Matta, M. Mircea, S. Fuzzi, A. R. Chughtai, and D. M. Smith (2002), Water soluble organic compounds formed by oxidation of soot, *Atmos. Environ.*, *36*, 1827–1832.

Dick, W. D., P. J. Ziemann, P. F. Huang, and P. H. McMurry (1998), Optical shape fraction measurements of submicrometre laboratory and atmospheric aerosols, *Measure. Sci. Technol.*, *9*(2), 183–196.

Draxler, R. R., and G. D. Rolph (2003), HYSPLIT (HYbrid Single-Particle Lagrangian Integrated Trajectory) model, NOAA Air Resour. Lab., Silver Spring, Md. (Available at http://www.arl.noaa.gov/ready/hysplit4.html)

Ebert, M., S. Weinbruch, A. Rausch, G. Gorzawski, G. Helas, P. Hoffmann, and H. Wex (2002), Complex refractive index of aerosols during LACE 98 as derived from the analysis of individual particles, *J. Geophys. Res.*, *107*(D21), 8121, doi:10.1029/2000JD000195.

Gelencsér, A., A. Hoffer, Z. Krivácsy, G. Kiss, A. Molnár, and E. Mészáros (2002), On the possible origin of humic matter in fine continental aerosol, *J. Geophys. Res.*, *107*(D12), 4137, doi:10.1029/2001JD001299.

Gucker, F. T., J. Tuma, H. M. Lin, C. M. Huang, S. C. Ems, and T. R. Marshall (1973), Rapid measurement of light-scattering diagrams from single aerosol particles in an aerosol stream and determination of the latex particle size, *Aerosol Sci.*, *4*, 389–404.

Hahn, D. W. (1998), Laser-induced breakdown spectroscopy for sizing and elemental analysis of discrete aerosol particles, *Appl. Phys. Lett.*, *72*, 2960–2962.

Hill, S. C., A. C. Hill, and P. W. Barber (1984), Light scattering by size shape distributions of soil particles, *Appl. Opt.*, *23*(7), 1025–1031.

Hirst, E., and P. H. Kaye (1996), Experimental and theoretical light scattering profiles from spherical and nonspherical particles, *J. Geophys. Res.*, *101*(D14), 19,231–19,235.

Hirst, E., P. H. Kaye, R. S. Greenaway, P. Field, and D. W. Johnson (2001), Discrimination of micrometre-sized ice and super-cooled droplets in mixed-phase cloud, *Atmos. Environ.*, *35*(1), 33–47.

Huang, P.-F., B. J. Turpin, M. H. Pipho, D. B. Kittelson, and P. H. McMurry (1994), Effects of water condensation and evaporation on diesel chain-agglomerate morphology, *J. Aerosol Sci.*, *25*(3), 447–459.

Jaenicke, R. (2005), Abundance of cellular material and proteins in the atmosphere, *Science*, *308*, 73.

Kaye, P. H. (1998), Spatial light-scattering analysis as a means of characterizing and classifying non-spherical particles, *Measure. Sci. Technol.*, *9*, 141–149.

Kaye, P. H., E. Hirst, J. M. Clark, and F. Micheli (1992), Airborne particle-shape and size classification from spatial light-scattering profiles, *J. Aerosol Sci.*, *23*(6), 597–611.

Kiss, G., B. Varga, I. Galambos, and I. Ganszky (2002), Characterization of water-soluble organic matter isolated from atmospheric fine aerosol, *J. Geophys. Res.*, *107*(D21), 8339, doi:10.1029/2001JD000603.

Kopcewicz, B., C. Nagamoto, R. Parungo, J. Harris, J. Miller, H. Sievering, and J. Rosinski (1991), Morphological studies of sulfate and nitrate particles on the east coast of North America and over the North Atlantic Ocean, *Atmos. Res.*, *26*, 245–271.

Krivacsy, Z., et al. (2000), Study of humic-like substances in fog and interstitial aerosol by size-exclusion chromatography and capillary electrophoresis, *Atmos. Environ.*, *34*, 4273–4281.

Larson, T. V., N. C. Ahlquist, and R. E. Weiss (1982), Chemical speciation of sulfuric acid-ammonium sulfate particles using temperature and humidity controlled nephelometry, *Atmos. Environ.*, *16*, 1587–1590.

Lee, S.-H., D. M. Murphy, D. S. Thomson, and A. M. Middlebrook (2002), Chemical components of single particles measured with particle analysis by laser mass spectrometry (PALMS) during the Atlanta Supersite Project: Focus on organic/sulfate, lead, soot, and mineral particles, *J. Geophys. Res.*, *107*(D1), 4003, doi:10.1029/2000JD000011.

Lee, S.-H., D. M. Murphy, D. S. Thomson, and A. M. Middlebrook (2003), Nitrate and oxidized organic ions in single particle mass spectra during the 1999 Atlanta Supersite Project, *J. Geophys. Res.*, *108*(D7), 8417, doi:10.1029/2001JD001455.

Lim, H.-J., and B. J. Turpin (2002), Origins of primary and secondary organic aerosol in Atlanta; results of time-resolved measurements during the Atlanta supersite experiment, *Environ. Sci. Technol.*, *36*(21), 4489–4496.

Mamane, Y., J. L. Miller, and T. G. Dzubay (1986), Characterization of individual fly ash particles emitted from coal- and oil-fired power plants, *Atmos. Environ.*, *20*(11), 2125–2135.

Marshall, T. R., C. S. Parmenter, and M. Seaver (1976), Characterization of polymer latex aerosols by rapid measurement of 360 degree light-scattering patterns from individual particles, *J. Colloid Interface Sci.*, *55*(3), 624–636.

Mukai, A., and Y. Ambe (1986), Characterization of humic acid-like brown substance in airborne particulate matter and tentative identification of its origin, *Atmos. Environ.*, *20*, 813–819.

Murphy, D. M., A. M. Middlebrook, and M. Warshawsky (2003), Cluster analysis of data from the particle analysis by laser mass spectrometry (PALMS) instrument, *Aerosol Sci. Technol.*, *37*, 382–391.

Novakov, T., and J. E. Penner (1993), Large contribution of organic aerosols to cloud condensation nuclei concentrations, *Nature*, *365*, 823–826.

Novakov, T., D. A. Hegg, and P. V. Hobbs (1997), Airborne measurements of carbonaceous aerosols on the east coast of the United States, *J. Geophys. Res.*, *102*(D25), 30,023–30,030.

Odum, J. R., T. Hoffmann, F. Bowman, D. Collins, R. C. Flagan, and J. H. Seinfeld (1996), Gas/particle partitioning and secondary organic aerosol yields, *Environ. Sci. Technol.*, *30*, 2580–2585.

Pan, Y. L., S. Holler, R. K. Chang, S. C. Hill, R. G. Pinnick, S. Niles, and J. R. Bottiger (1999), Single-shot fluorescence spectra of individual micrometer-sized bioaerosols illuminated by a 351- or a 266-nm ultraviolet laser, *Opt. Lett.*, *24*(2), 116–118.

Pan, Y. L., K. B. Aptowicz, R. K. Chang, M. Hart, and J. D. Eversole (2003), Characterizing and monitoring respiratory aerosols by light scattering, *Opt. Lett.*, *28*(8), 589–591.

Pan, Y. L., V. Boutou, J. R. Bottiger, S. S. Zhang, J.-P. Wolf, and R. K. Chang (2004), A putt of air sorts bioaerosols for pathogen identification, *Aerosol Sci. Technol.*, *38*, 598–602.

Pinnick, R. G., G. Fernandez, B. D. Hinds, C. W. Bruce, R. W. Schaefer, and J. D. Pendleton (1985), Dust generated by vehicular traffic on unpaved roadways: Sizes and infrared extinction characteristics, *Aerosol Sci. Technol.*, *4*, 99–121.

Pinnick, R. G., S. G. Jennings, and G. Fernandez (1987), Volatility of aerosols in the southwestern United States, *J. Atmos. Sci.*, *44*(3), 562–576.

Pinnick, R. G., S. C. Hill, P. Nachman, J. D. Pendleton, G. L. Fernandez, M. W. Mayo, and J. G. Bruno (1995), Fluorescnce particle counter for detecting airborne bacteria and other biological particles, *Aerosol Sci. Technol.*, *23*, 653–664.

Pinnick, R. G., S. C. Hill, Y. L. Pan, and R. K. Chang (2004), Fluorescence spectra of atmospheric aerosol at Adelphi, Maryland, USA: Measurement and classification of single particles containing organic carbon, *Atmos. Environ.*, *38*(11), 1657–1672.

Pósfai, M., A. Gelencsér, R. Simonics, K. Arató, J. Li, P. V. Hobbs, and P. R. Buseck (2004), Atmospheric tar balls: Particles from biomass and biofuel burning, *J. Geophys. Res.*, *109*, D06213, doi:10.1029/2003JD004169.

Prather, K. A., T. Nordmeyer, and K. Salt (1994), Real-time characterization of individual aerosol particles using time-of-flight mass-spectrometry, *Anal. Chem.*, *66*, 1403–1407.

Press, W. H., S. A. Teukolsky, W. T. Vetterling, and B. P. Flannery (1992), *Numerical Recipes in Fortran 77: The Art of Scientific Computing*, chap. 15, pp. 678–683, Cambridge Univ. Press, New York.

Prospero, J. M., R. J. Charlson, V. Mohnen, R. Jaenicke, A. C. Delany, J. Moyers, W. Zoller, and K. Rahn (1983), The atmospheric aerosol system: An overview, *Rev. Geophys.*, *21*(7), 1607–1629.

Qian, G.-W., and Y. Ishizaka (1993), Electron microscope studies of methane sulfonic acid in individual aerosol particles, *J. Geophys. Res.*, *98*(C5), 8459–8470.

Rietmeijer, J. M., and J. Janeczek (1997), An analytical electron microscope study of airborne industrial particles in Sosnowiec, Poland, *Atmos. Environ.*, *31*(13), 1941–1951.

Rogge, W. F., M. A. Mazurek, L. M. Hildemann, and G. R. Cass (1993), Quantification of urban organic aerosols at a molecular level: Identification of abundance and seasonal variation, *Atmos. Environ., Part A*, *27*, 1309–1330.

Sachweh, B. A., W. D. Dick, and P. H. McMurry (1995), Distinguishing between spherical and nonspherical particles by measuring the variability in azimuthal light-scattering, *Aerosol Sci. Technol.*, *23*(3), 373–391.

Samuels, A. C., F. C. DeLucia, K. L. McNesby, and A. W. Miziolek (2003), Laser-induced breakdown spectroscopy of bacterial spores, molds, pollens, and protein: Initial studies of discrimination potential, *Appl. Opt.*, *42*(30), 6205–6209.

Saxena, P., and L. M. Hildemann (1996), Water-soluble organics in atmospheric particles: A critical review of the literature and application to thermodynamics to identify candidate compounds, *J. Atmos. Chem.*, *24*, 57–109.

Secker, D. R., P. H. Kaye, R. S. Greenaway, E. Hirst, D. L. Bartley, and G. Videen (2000), Light scattering from deformed droplets and droplets with inclusions, *Appl. Opt.*, *39*(27), 5023–5030.

Seinfeld, J. H., and S. N. Pandis (1998), *Atmospheric Chemistry and Physics: From Air Pollution to Climate Change*, Wiley-Interscience, Hoboken, N. J.

Shaffer, B. T., and B. Lighthart (1997), Survey of culturable airborne bacteria at four diverse locations in Oregon: Urban, rural, forest, and coastal, *Microbial Ecol.*, *34*, 167–177.

Sheridan, P. J., R. C. Schnell, J. D. Kahl, J. F. Boatman, and D. M. Garvey (1993), Microanalysis of the aerosol collected over south-central New Mexico during the ALIVE field experiment, May–December 1989, *Atmos. Environ., Part A*, *27*, 1169–1183.

Sullivan, R. C., and K. A. Prather (2005), Recent advances in our understanding of atmospheric chemistry and climate made possible by on-line aerosol analysis instrumentation, *Anal. Chem.*, *77*, 3861–3886.

Tang, I. N. (1976), Phase transformation and growth of aerosol particles composed of mixed salts, *J. Aerosol Sci.*, *7*(5), 361–371.

Tang, I. N., and R. R. Munkelwitz (1977), Aerosol growth studies—III. Ammonium bisulfate aerosols in a moist atmosphere, *J. Aerosol Sci.*, *8*(5), 321–330.

Tang, I. N., R. R. Munkelwitz, and J. G. Davis (1977), Aerosol growth studies—II. Preparation and growth measurements of monodisperse salt aerosols, *J. Aerosol Sci.*, *8*(3), 149–159.

Videen, G., W. Sun, Q. Fu, D. R. Secher, R. S. Greenaway, P. H. Kaye, E. Hirst, and D. Bartley (2000), Light scattering from deformed droplets and droplets with inclusions. II Theoretical treatment, *Appl. Opt.*, *39*(27), 5031–5039.

Weiss, R. E., A. P. Waggoner, R. J. Charlson, and N. C. Ahlquist (1977), Sulfate aerosol: Its geographic extent in the midwestern and southern United States, *Science*, *195*, 979–981.

Wyatt, P. J., K. L. Schehrer, S. D. Phillips, C. Jackson, Y. J. Chang, R. G. Parker, D. T. Phillips, and J. R. Bottiger (1988), Aerosol-particle analyzer, *Appl. Opt.*, *27*(2), 217–221.

Zappoli, S., et al. (1999), Inorganic, organic and macromolecular components of fine aerosol in different areas of Europe in relation to their water solubility, *Atmos. Environ.*, *33*, 2733–2743.

K. B. Aptowicz, Department of Physics, West Chester University, West Chester, PA 19383, USA. (kaptowicz@wcupa.edu)

R. K. Chang and Y. L. Pan, Department of Applied Physics and Center for Laser Diagnostics, Yale University, New Haven, CT 06520-8284, USA.

S. C. Hill and R. G. Pinnick, U.S. Army Research Laboratory, Adelphi, MD 20783, USA.